

Properties of amorphous Zr_3RhH_x prepared from glassy and crystalline alloys

R. C. Bowman, Jr.

Chemistry and Physics Laboratory, The Aerospace Corporation, P.O. Box 92957, Los Angeles, California 90009-2957

J. S. Cantrell

*Department of Chemistry, Miami University, Oxford, Ohio 45056
and Mound Laboratory, Monsanto Research Corporation, Miamisburg, Ohio 45342*

K. Samwer and J. Tebbe

I. Physikalisches Institut der Universität Göttingen, D-3400 Göttingen, Federal Republic of Germany

E. L. Venturini

Sandia National Laboratories, Albuquerque, New Mexico 87185

J. J. Rush

National Bureau of Standards, Gaithersburg, Maryland 20899

(Received 12 November 1987)

The electronic, magnetic, and thermal properties have been measured on the amorphous hydride phases prepared from originally glassy or crystalline Zr_3Rh alloys. The a - Zr_3RhH_x samples with $x \leq 5.5$ were studied by x-ray diffraction, proton nuclear magnetic resonance, magnetic susceptibility, low-temperature heat capacity, differential scanning calorimetry, and inelastic neutron scattering. All hydride samples are amorphous with similar properties which are shown to be independent of the structure for the initial alloy. Namely, the solid-state reaction of hydrogen with crystalline c - Zr_3Rh appeared to produce an equivalent amorphous phase to hydrogenated glassy alloys. The changes in the electronic and magnetic properties upon hydrogenation imply a systematic decrease in the Fermi-level density of states in a - Zr_3RhH_x as the hydrogen content x increases. The thermal stabilities of the amorphous hydrides (with respect to the irreversible formation of crystalline ZrH_x phases) also decrease with increasing hydrogen stoichiometry. Whereas the hydrogen atoms predominantly occupy tetrahedral interstitial sites coordinated with zirconium atoms, there is strong circumstantial evidence for occupancies of different and less stable sites for compositions with higher hydrogen content.

I. INTRODUCTION

Within the past few years there has been considerable interest in the behavior of hydrogen in amorphous metallic alloys.¹ Significant differences in the hydrogen-absorption capacity, isotherms, electronic properties, magnetic character, embrittlement tendencies, and hydrogen-diffusion parameters have been found between amorphous hydrides and corresponding crystalline hydride phases. Much attention has been directed on the effects of hydrogen in the zirconium-based metallic glasses a - Zr_yB_{1-y} where B corresponds to the late transition metals Fe, Ni, Cu, Rh, or Pd. This interest has been stimulated by the relative ease by which these metallic glasses can be produced over wide composition ranges by conventional rapid-quenching methods² as well as their ability to absorb large quantities of hydrogen (e.g., hydrogen-to-metal ratios often exceed unity for $y \geq 0.5$) without crystallization.³⁻⁵ Furthermore, direct comparisons between hydrides formed from crystalline and glassy alloys with identical metal-atom compositions have been possible in some cases.^{4,6,7}

The properties of the a - Zr_3RhH_x system have been ex-

tensively studied by the present authors,⁷⁻¹⁵ while other workers¹⁶⁻¹⁸ have recently reported additional information on the formation and stability of a - $Zr_yRh_{1-y}H_x$ for $0.75 \leq y \leq 0.85$. One factor for all of this attention is that the production of a - Zr_3RhH_x from the metastable crystalline Zr_3Rh alloy was the first example⁸ of the solid-state-reaction (SSR) process that has been subsequently used to create amorphous phases from various crystalline materials.^{19,20} Successful amorphization by SSR requires¹⁴ (1) a large negative heat of mixing to provide a thermodynamically favorable process, and (2) greatly enhanced mobility for one of the atomic species while the other species remain sufficiently immobile to prevent segregation of more stable crystalline phases. Much effort has been made to experimentally establish^{8,11,14,16,18} that amorphous a - Zr_3RhH_x produced by SSR is equivalent to the hydride formed when initially glassy a - Zr_3Rh alloy absorbs hydrogen gas.

The intent of this paper is to provide a comprehensive assessment of various properties of amorphous a - Zr_3RhH_x samples that had been prepared from rapidly quenched amorphous and crystalline alloys. Although a major emphasis will be to demonstrate that SSR hydro-

genation of metastable crystalline Zr_3Rh produces an essentially identical amorphous hydride to that which is formed directly from glassy $a-Zr_3Rh$ alloys, the influence of hydrogen concentration on electrical, magnetic, and crystallization properties will be described. In light of new experimental data from differential-scanning-calorimetry (DSC), x-ray-diffraction (XRD), proton nuclear-magnetic-resonance (NMR), magnetic-susceptibility, low-temperature specific-heat (C_p), and inelastic-neutron-scattering measurements, some clarifications and corrections will be made to previous interpretations⁸⁻¹⁸ on the crystalline structure, electronic structure, and thermal stabilities of $a-Zr_3RhH_x$. Detailed discussions of hydrogen diffusion from NMR studies^{7,10} will be treated separately.²¹

II. EXPERIMENTAL METHODS AND RESULTS

A. Sample preparation and composition

Stoichiometric mixtures of the metals Zr and Rh were initially melted together on a silver boat in a gettered argon atmosphere. These Zr_3Rh ingots were rapidly quenched by either the melt-spinning (MS) or anvil-piston (AP) techniques as previously described.^{8,22,23} Some properties for a few of these alloys are given in Table I. All of the Zr_3Rh alloys listed in Table I, except sample R-AP-C (R denotes an alloy that contains rhodium), were found by x-ray diffraction to be amorphous after quenching. However, alloy R-AP-C was shown⁸ to be crystalline with a metastable cubic $L1_2$ structure. The densities, ρ , for the amorphous alloys in Table I are equal within error to the value 7.57(1) g/cm³ given by Drehman and Johnson²² for stoichiometric $a-Zr_3Rh_{25}$. Some additional properties of these samples, such as their superconducting transition temperature (T_{sc}), linear coefficient of resistivity, and crystallization parameters, have been reported earlier.^{8,10,11,13,23}

The amorphous hydrides $a-Zr_3RhH_x$ were prepared by direct reactions with hydrogen gas. To prevent accidental crystallization³ during hydrogenation, the temperatures were held below 485 K. Reaction times varied between several days for the AP alloys^{8,9,11} and 6 weeks for the MS alloys¹³ before the hydrogen absorptions were deemed to be complete. While nominal hydride compositions could be estimated from volumetric differences in hydrogen gas during synthesis or mass increases of the alloys, there was evidence¹³ for inhomogeneous reactions with approximately 10–20 % of the glasses absorbing little or no hydrogen. Consequently, nondestructive proton NMR spin counts^{10,24} were used to determine the stoichiometries of several $a-Zr_3RhH_x$ powders and are presented in Table I. More accurate determinations of compositions were obtained in a few cases by the destructive thermal-desorption (TD) volumetric method¹³ and are also given in Table I.

B. Magnetic properties

The bulk magnetic susceptibilities $\chi_m(T)$ of the $a-Zr_3RhH_x$ samples were obtained from least-squares fits to

TABLE I. Summary of experimental properties for metallic glasses $a-Zr_3Rh$ and amorphous ternary hydrides $a-Zr_3RhH_x$ (see text for parameter descriptions). (comp. denotes composition.)

Nominal sample comp.	Alloy source	Sample form	ρ (g/cm ³)	Meas. x NMR	TD	[H]/[M]	$\chi_p(0)$ (10^{-6} cm ³ /g)	B (10^{-6} K ⁻²)	C (10^{-6} cm ³ K/g)	T_{sc} (K)	Θ_D (K)	$(T_1 T)^{-1/2}$ (s K) ^{-1/2}	$N_\gamma(E_F)$ (states/eV atom)	T_{exo} (K)	T_{endo} (K)
$a-Zr_3Rh$	R-MS-1	ribbon	7.56(8)			0	1.25	0.56	0.54	4.50 ^c				734,855	
$a-Zr_3Rh$	R-MS-2	ribbon	7.53(5)			0	1.23	0.46	0.01	4.55 ^c				731,856	
$a-Zr_3Rh$	R-MS-3	ribbon	7.50(12)			0	1.32	0.39	0.33					716,771	
$a-Zr_3Rh$	R-AP-1	foil	7.58 ^a			0	1.10	0.39	0.09	4.40 ^a	191 ^b		2.43 ^b	716,791	> 900
$a-Zr_3RhH_{3.7}$	R-MS-3	powder		3.7(1)		0.92						0.0685		649	
$a-Zr_3RhH_{3.6}$	R-MS-2	ribbon				0.90	0.85	-0.07	-0.25	2.95 ^c	258(13)		0.85(16)	652,705,774	
$a-Zr_3RhH_{4.4}$	R-MS-2	powder		4.1(2)	4.40	1.10	0.68	0.58	0.25					658	> 874
$a-Zr_3RhH_{5.0}$	R-AP-2	powder	6.54 ^a	5.0(2)		1.25				1.21 ^b	347 ^b		0.54 ^b	608(1)	673(12)
$a-Zr_3RhH_{5.1}$	R-AP-3	powder		5.1(2)		1.28								616(2)	638
$a-Zr_3RhH_{5.2}$	R-AP-4	powder		5.2(4)		1.30	0.55	0.45	1.05						
$a-Zr_3RhH_{5.45}$	R-AP-5	powder		4.9(3)	5.45	1.36	0.52	0.32	1.68						555(15)
$a-Zr_3RhH_{5.3}$	R-AP-C ^d	powder	6.53 ^a	5.2(4)	5.31	1.33	0.62	0.61	0.32	1.03 ^b	379 ^b	0.0694	0.58	616(1)	695

^aData from Samwer and Johnson (Ref. 9).

^bData from Tebbe *et al.* (Ref. 11).

^cData from Bowman *et al.* (Ref. 10).

^dCrystalline $L1_2$ structure for alloy prior to reaction with H₂ gas to form amorphous hydride.

the magnetizations measured for magnetic fields up to 20 kG with a Biotechnology Corporation S.H.E. magnetometer as previously described.¹² These measurements were performed over the temperature range 7–300 K. The $\chi_m(T)$ results for the a - Zr_3Rh alloys and amorphous hydrides are presented in Fig. 1 and Fig. 2, respectively. Since these samples exhibit Pauli paramagnetism, the phenomenological expression²⁵

$$\chi_m(T) = \chi_p(0)(1 + BT^2) + C/T \quad (1)$$

has been used to describe the temperature dependencies of the magnetic susceptibility. The parameter $\chi_p(0)$ is the temperature-independent Pauli susceptibility plus diamagnetic and orbital contributions,^{12,25} B is the Pauli temperature-dependent term, which is relatively small for the a - Zr_3RhH_x samples, and C is an empirical Curie-like component due to magnetic impurities²⁵ that only affects $\chi_m(T)$ at temperatures below about 40 K in the worst cases. Summaries of the magnetic parameters $\chi_p(0)$, B , and C from least-squares fits to the magnetic-susceptibility data in Figs. 1 and 2 are given in Table I. For a couple of samples, slightly better fits were obtained¹² with a linear temperature coefficient B ; however, the improvement was actually quite small and the more common²⁵ quadratic form in Eq. (1) has been chosen for the present work. Furthermore, the $\chi_m(T)$ values for a - Zr_3RhH_x are only very weakly temperature dependent and little (if any) physical insights can be derived from the B and C magnetic parameters.

The $\chi_m(T)$ data for the glassy a - Zr_3Rh alloys exhibit an approximately 25% variation which cannot be readily attributed to differences in composition since their stoichiometries are essentially identical,²³ with the possible exception of sample R -AP-1, whose value remains somewhat uncertain. These alloys had also showed remarkable differences in their crystallization behavior,^{13,23} which has been tentatively associated with different degrees of chemical short-range order (CSRO) produced

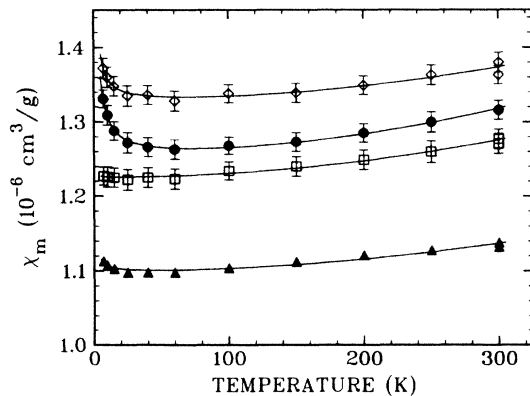


FIG. 1. Temperature dependencies of the magnetic susceptibilities for a - Zr_3Rh metallic glasses: ●, R -MS-1; □, R -MS-2; ◇, R -MS-3; ▲, R -AP-1 (see Table I for additional information). The curves correspond to fits with Eq. (1) and the parameters in Table I.

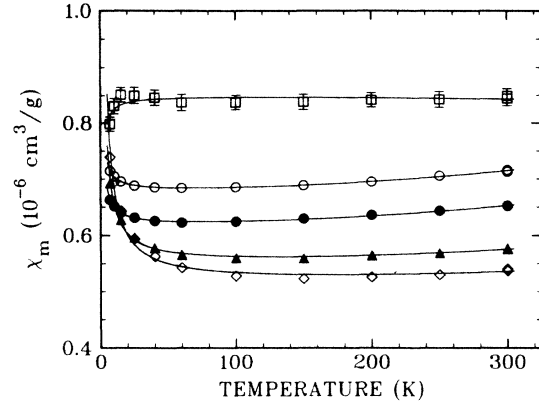


FIG. 2. Temperature dependencies of the magnetic susceptibilities for amorphous hydrides: □, a - $Zr_3RhH_{3.6}$ (ribbon); ○, a - $Zr_3RhH_{4.4}$ (powder); ▲, a - $Zr_3RhH_{5.2}$; ◇, a - $Zr_3RhH_{5.45}$; ●, a - $Zr_3RhH_{5.3}$ (originally crystalline alloy). The curves are fits to Eq. (1) as for Fig. 1.

during the rapid-quenching process used to form the glasses. It is possible that CSRO differences can also be reflected in the magnetic properties as well. Furthermore, the only other $\chi_m(T)$ data for a similar paramagnetic amorphous Zr-Rh alloy are given by Eifert *et al.*,²⁶ who reported $\chi_m \approx 2.5 \times 10^{-6} \text{ cm}^3/\text{g}$ for a - $Zr_{0.74}Rh_{0.26}$, which is almost exactly twice as large as the values in Fig. 1. It seems very unlikely that a 1% difference in Rh content could cause this large change in magnetic susceptibility. However, differences in CSRO arising from the alloy-preparation conditions could be partially responsible. Of course, the more likely contributions of impurities either initially present in the metals or introduced during processing could be significant as previously observed²⁵ in ZrH_x and cannot be completely eliminated without chemical analyses of these alloys.

As has been previously observed,^{10,12} Fig. 2 clearly shows that hydrogen absorption causes the magnetic susceptibility of a - Zr_3RhH_x to substantially decrease. This behavior will be discussed more thoroughly in a later section of the paper. The $\chi_m(T)$ data for the originally crystalline a - $Zr_3RhH_{5.3}$ lie above the values for the originally amorphous alloy a - $Zr_3RhH_{5.2}$. However, differences in the magnetic susceptibilities of the original Zr_3Rh alloys may be responsible since CSRO should not be identical between the crystalline and glassy phases. Unfortunately, $\chi_m(T)$ for the crystalline alloy R -AP-C was not measured prior to the reaction with hydrogen to produce the amorphous hydride.

C. Proton nuclear magnetic resonance

The proton spin-lattice-relaxation times (T_1) have been shown to provide novel information on the electronic structures of crystalline and amorphous metal hydrides^{7,27} that complement band-structure calculations and the more conventional experimental approaches such as specific heat, magnetic susceptibility, and photoemission spectroscopy. In particular, the conduction-electron contribution (T_{1e}) to proton spin-lattice relaxation in

transition-metal systems corresponds to the Fermi density of electronic states, $N(E_F)$, through the generalized^{7,27} Korringa relation

$$(T_{1e}T)^{-1} = C_\gamma \{ [H_{\text{hf}}(s)N_s(E_F)]^2 + q [H_{\text{hf}}(d)N_d(E_F)]^2 \} . \quad (2)$$

Here, C_γ is a numerical factor for the specific spin (e.g., protons), q is the well-known²⁸ d -orbital-degeneracy factor, $N_s(E_F)$ and $N_d(E_F)$ are the unscreened s - and d -band density of electron states at the Fermi level without electron-phonon enhancement, respectively, $H_{\text{hf}}(s)$ is the positive Fermi-contact hyperfine field produced by the unpaired s -state electrons, and $H_{\text{hf}}(d)$ is the negative hyperfine field due to polarization of spin-paired hydrogen s -state orbitals in the valence band that arise from the unpaired Fermi-level d electrons of the transition metals. While $H_{\text{hf}}(s) \gg H_{\text{hf}}(d)$, the large $N_d(E_F)$ values in most transition-metal hydrides usually cause the polarization term to dominate Eq. (2). However, proton spin-lattice relaxation also has other contributions due to either diffusion processes^{7,27} or fluctuating magnetic fields from paramagnetic impurities.²⁹ If the material under study is free of magnetic impurities (which is the situation for the three $a\text{-Zr}_3\text{RhH}_x$ samples used in this work), the proton T_{1e} values can usually be determined by measuring the spin-lattice-relaxation times at sufficiently low temperature where diffusion contributions become negligible.^{7,27}

Proton T_1 measurements at a 34.5-MHz resonance frequency were performed on three $a\text{-Zr}_3\text{RhH}_x$ samples by the inversion-recovery method³ for temperatures between 100 and 300 K. Unfortunately, there were not adequate quantities of the other $a\text{-Zr}_3\text{RhH}_x$ powder preparations to permit reliable measurements of their T_1 values with the available equipment. For temperatures below 150 K, the proton T_1 data obeyed the empirical relation $T_1T = C_K$, where C_K is a constant. This behavior implies that diffusion processes were not contributing to the proton spin-lattice relaxation at these temperatures. The mean values of the $(T_1T)^{-1/2}$ parameters, which are related to the average density of Fermi-level states according to Eq. (2), obtained at temperatures below 160 K are summarized in Table I. It is interesting to note that the proton $(T_1T)^{-1/2}$ parameters appear to be nearly independent of hydrogen content over the range $3.7 \leq x \leq 5.3$. The impact of this behavior on the nature of the $a\text{-Zr}_3\text{RhH}_x$ electronic structure will be discussed later in the paper.

D. Inelastic neutron scattering

The optical vibrational frequencies of hydrogen in metals can be readily determined from inelastic-neutron-scattering (INS) measurements.^{30,31} The properties of these INS spectra (e.g., peak frequencies, relative intensities, and linewidths) can be directly related³¹ to the local potentials and lattice-site occupancies of the hydrogen atoms. While most INS experiments have been performed on crystalline metal hydrides,^{30,31} hydrogen INS spectra have been obtained from amorphous hydrides^{4,32,33} since the first comparison of the vibrational

spectra for crystalline and glassy TiCuH_x by Rush *et al.*³⁴ The vibrational spectra from the metallic glass hydrides are always considerably wider than the spectra from corresponding crystalline hydrides, although the peak positions are virtually identical for both phases. Hence, the INS spectra infer similar hydrogen-site occupancies, but with a greater range of local environments in the glassy hydrides from their inherent topological disorder.³²⁻³⁴

The hydrogen vibration spectrum of $a\text{-Zr}_3\text{RhH}_{3.7}$ was obtained by room-temperature INS measurements at the National Bureau of Standards BT-4 triple-axis spectrometer equipped with a Be-filter analyzer.³⁵ The spectrum is shown in Fig. 3, and various derived parameters are summarized in Table II along with similar data from INS measurements on other glassy Zr-based hydrides³⁶⁻³⁸ as well as crystalline ϵ -phase (i.e., tetragonal) $\text{ZrH}_{2.0}$ (Ref. 39). As was previously observed in other glassy-metal hydrides,^{32,34} the hydrogen INS spectra parameters in Table II for the amorphous Zr glasses all have broad linewidths [i.e., full width at half maxima (FWHM) exceed 50 meV] and peaks near the position of the 140-meV maximum for crystalline $\text{ZrH}_{2.0}$. Since hydrogen occupies tetrahedral sites^{30,40} in $\epsilon\text{-ZrH}_{2.0}$, the INS parameters indicate most hydrogen atoms in the glassy hydrides also reside on tetrahedral sites, albeit with considerable distortion or substitution^{2,32-34} to produce the large FWHM values. However, the spectrum in Fig. 2 also has considerable intensity at energies below 100 meV, which is the region for vibrations of hydrogen in octahedral sites.³⁰ Hence some (i.e., $\leq 10\%$) of the hydrogen atoms in $a\text{-Zr}_3\text{RhH}_{3.7}$ may be in octahedral sites. Similar conclusions were obtained from the INS spectra for $a\text{-TiCuH}_{1.3}$ (Ref. 34) and $a\text{-Ti}_2\text{NiH}_{1.5}$ (Ref. 2). However, Williams, *et al.*³⁶ stated that hydrogen occupies only tetrahedral sites in their $a\text{-Zr}_2\text{PdH}_{3.0}$ sample.⁴¹

Because the $a\text{-Zr}_3\text{RhH}_{3.7}$ sample had the largest mass (e.g., about 0.5 g), it was not practical to obtain INS spectra from the other $a\text{-Zr}_3\text{RhH}_x$ preparations which were only available in amounts less than 0.2 g. Hence, the interesting possibility of changes in hydrogen-site occupancy at the higher stoichiometries could not be determined from INS measurements of the hydrogen vibration spectra.

E. Low-temperature specific heat

The specific heat (C_p) of several $a\text{-Zr}_3\text{RhH}_x$ alloys at low temperature (i.e., $1.5 < T < 9$ K) was measured by a modified heat-pulse technique in a standard helium cryostat.⁴² Using a sapphire plate with the heater and thermometer attached on one side, the mass of the sample mounted on the opposite side can be as small as 40 mg. The conventional expression for the specific heat,

$$C_p/T = \gamma + \beta T^2 ,$$

provides the phonon-dressed density of states, $N_\gamma(E_F)$, and Debye temperature (Θ_D) from the parameters γ and β , respectively. Furthermore, the superconductivity transition of the alloy can be clearly seen by a jump in the

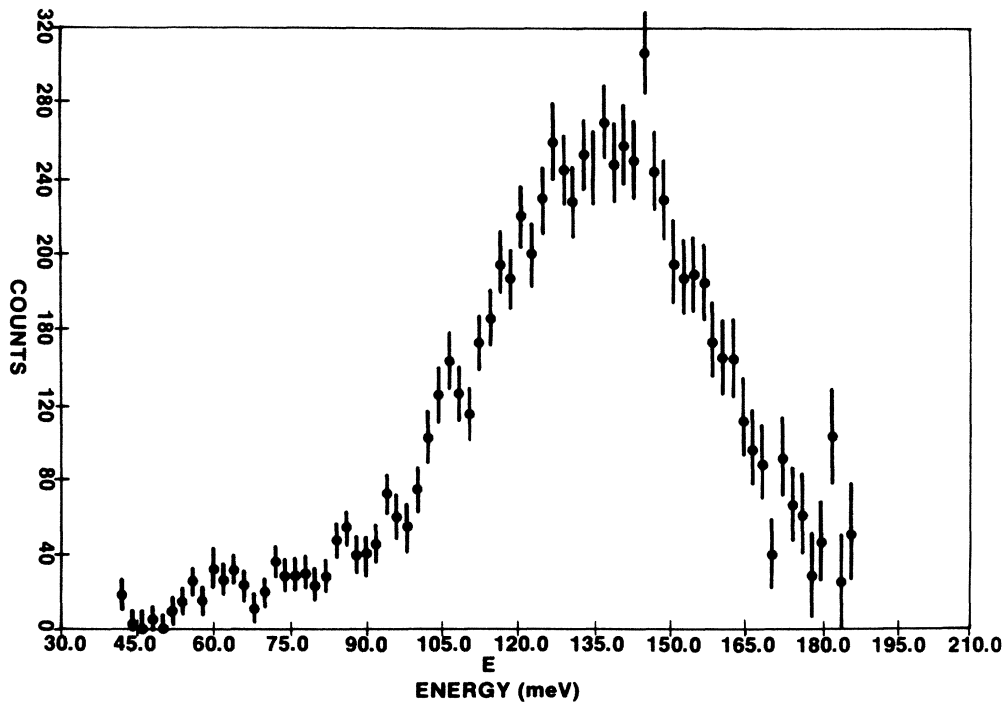


FIG. 3. Room-temperature inelastic-neutron-scattering spectrum from a - $Zr_3RhH_{3.7}$ powder sample.

specific heat at the critical temperature T_{sc} . Plots of Eq. (3) for two of the a - Zr_3RhH_x samples have been previously reported^{11,14} while new C_p experiments were performed on ribbon pieces of a - $Zr_3RhH_{3.6}$. The Θ_D and $N_\gamma(E_F)$ values are summarized in Table I.

F. Calorimetry and x-ray-diffraction studies

The crystallization behavior of glassy a - Zr_3RhH_x has been monitored by differential scanning calorimetry (DSC) and powder x-ray diffraction (XRD). Although detailed descriptions of these techniques and the measurement procedures have been given,^{13,23} a brief summary will be presented. The glassy alloy or hydride sam-

ples were accurately weighed into gold DSC cups which were subsequently hermetically sealed under purified argon gas. The DSC experiments were performed on Perkin-Elmer model DSC-2 calorimeters. All the DSC results presented in this paper were obtained with 20-(K/min) heating rates. However, some a - Zr_3RhH_x alloys had been heated at several different heating rates to determine the crystallization activation energies.¹³ Powder XRD data were obtained with Philips-Norelco and Rigaku diffractometers operating in the θ - 2θ scan modes for Cu $K\alpha$ radiation. The individual DSC samples were specially handled^{13,23} to obtain their XRD patterns with maximum sensitivity. The DSC runs were often halted at intermediate temperatures (i.e., usually just

TABLE II. Central peak positions, half maximum (FWHM) linewidths, and high-energy-low-energy asymmetry parameter (Γ_{HL}) for hydrogen vibrational spectra from inelastic-neutron-scattering measurement on amorphous Zr-based hydride and crystalline ϵ -phase (tetragonal) $ZrH_{2.00}$.

Material	[H]/[M]	T (K)	Peak (meV)	FWHM (meV)	Γ_{HL}	Data source
a - $Zr_3RhH_{3.7}$	0.92	295	136(2)	52(5)	0.89(4)	Present work
a - $Zr_2PdH_{3.0}$	1.00	10	125(3)	62(3)	1.01(2)	Williams <i>et al.</i> ^b
a - $ZrNiH_{1.8}$	0.90	298	130(3)	70(5)	0.85(5)	H. Kaneko <i>et al.</i> ^c
a - $Zr_2NiH_{4.4}$	1.47	298	129(5)	61(5)	0.93(5)	H. Kaneko <i>et al.</i> ^c
a - $Zr_{76}Fe_{24}H_{173}$	1.73	295	137(4)	63(6)	0.97(5)	Rush <i>et al.</i> ^d
ϵ - $ZrH_{2.00}$ ^a	2.00	296	140(1)	21(1)		Couch <i>et al.</i> ^e

^aFigure 2 of Ref. 39 clearly indicates fine structure at 137, 143, and 154 meV in the optical vibrational peak.

^bReference 36.

^cReference 37.

^dReference 38.

^eReference 39.

above or below a major transition peak) to permit x-ray identification of the phases present at the temperature (T_{\max}) from which the sample had been quenched.

The DSC-XRD experiments were performed on all the samples listed in Table I except $a\text{-Zr}_3\text{RhH}_{5.2}$ (*R*-AP-4). Representative DSC traces are presented in Figs. 4–6, while additional examples can be found in earlier papers.^{10,13,23} As illustrated in Fig. 4, both exothermic and endothermic transitions with peak temperatures denoted T_{exo} and T_{endo} , respectively, have been obtained. The observed T_{exo} and T_{endo} values for the $a\text{-Zr}_3\text{RhH}_x$ samples are summarized in Table I. The endothermic peaks are seen to completely obscure the exothermic transitions in $a\text{-Zr}_3\text{RhH}_{5.45}$. The DSC traces for glassy $a\text{-Zr}_3\text{Rh}$ alloy (*R*-MS-2) and as-reacted foil pieces (i.e., $a\text{-Zr}_3\text{RhH}_{3.6}$) and sieved powder (i.e., $a\text{-Zr}_3\text{RhH}_{4.4}$) ground from these hydrided ribbons are compared in Fig. 5. Substantial differences in the exothermic peaks are quite apparent that are also reflected in the crystallization products detected in the subsequent XRD measurements, as will be discussed later in this section.

The great similarity of the amorphous $a\text{-Zr}_3\text{RhH}_5$ samples produced from glassy alloy (*R*-AP-2) and originally

crystalline alloy (*R*-AP-C) is shown by the DSC traces in Fig. 6. The T_{exo} values are nearly identical, while the differences in the T_{endo} peaks are not especially great since the variability of this latter transition between individual DSC runs often approached 30 K. Furthermore, the mean exothermic heats of crystallization (ΔH_{exo}) are $-14.1(12)$ kJ/g-atom-metal (Ref. 43) for $a\text{-Zr}_3\text{RhH}_{5.0}$ (*R*-AP-2) and $-13.7(2)$ kJ/g-atom-metal for $a\text{-Zr}_3\text{RhH}_{5.3}$ from the originally crystalline alloy (*R*-AP-C). Hence, both samples released essentially identical energies upon crystallization. Additional evidence for the independence of the amorphous $a\text{-Zr}_3\text{RhH}_x$ hydride phase from the initial structure of the alloy is provided by portions of the XRD patterns presented in Figs. 7 and 8. Prior to the DSC measurements, broad diffraction peaks indicative^{3,9} of the glassy state are predominant, except for weak peaks from ZrO_2 , which probably represent a surface oxide formed after several months exposure of the hydrided foils to air. The XRD patterns obtained from both samples at temperatures immediately above the exothermic transitions (i.e., $T_{\max} \approx 650$ K) show strong peaks at the 2θ value 32.4° , which corresponds to the strongest diffraction peak²⁵ of the cubic (δ) and tetragonal (ϵ)

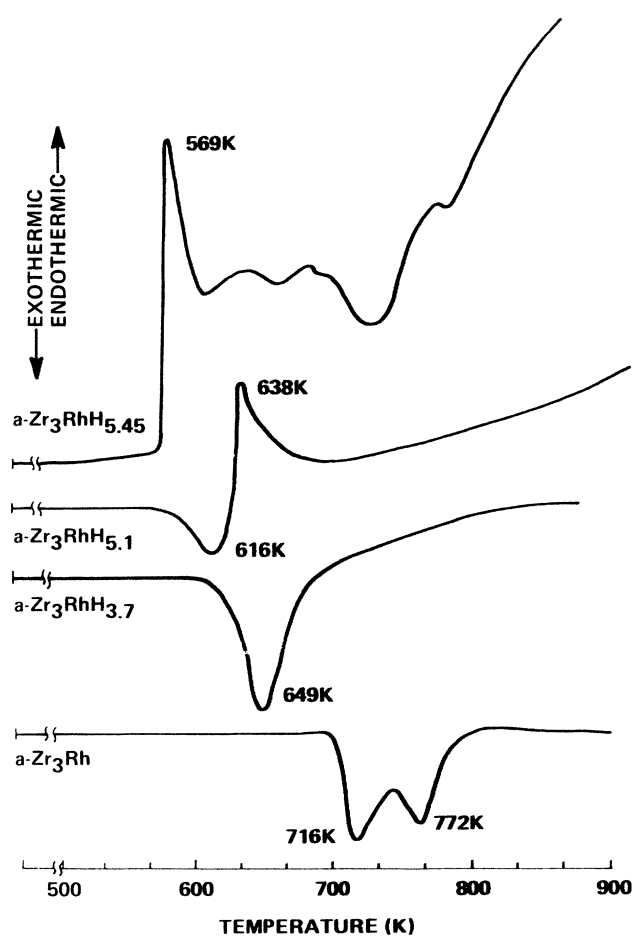


FIG. 4. Representative DSC traces at 20 K/min for the glassy alloy $a\text{-Zr}_3\text{Rh}$ (*R*-MS-3) and three amorphous hydrides $a\text{-Zr}_3\text{RhH}_x$.

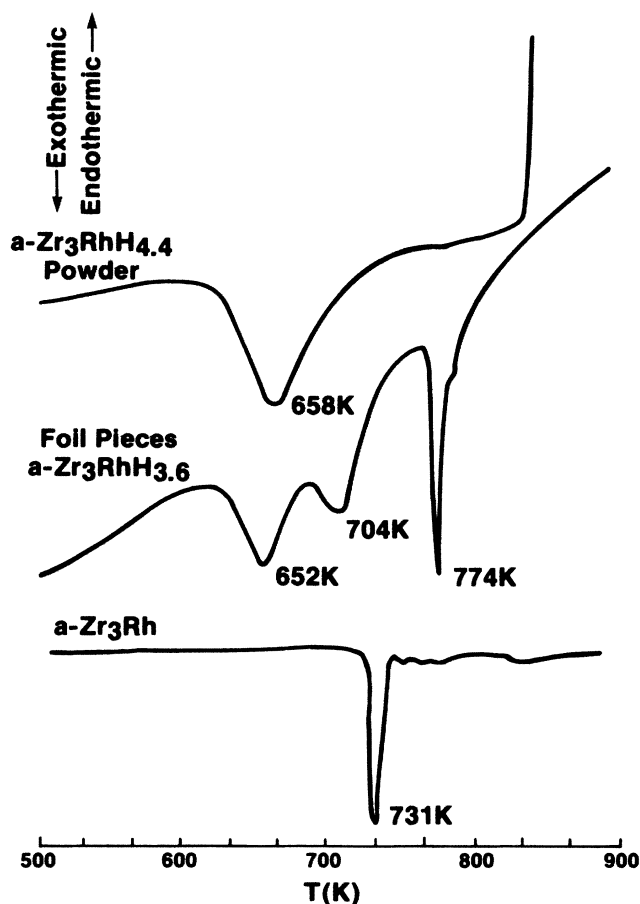


FIG. 5. Comparison of 20-(K/min) DSC traces for glassy $a\text{-Zr}_3\text{Rh}$ alloy (*R*-MS-2) and unground (i.e., foil pieces) and powder samples of the amorphous hydride $a\text{-Zr}_3\text{RhH}_x$ prepared from this glass.

phases of ZrH_x when $x > 1.5$. Additional heating up to 900 K causes some further sharpening of the XRD lines for both samples, but no peaks clearly assignable to other phases. The phase identifications for a large number of DSC-heated $a-Zr_3RhH_x$ samples are summarized in Table III. Although the different batches of glassy $a-Zr_3Rh$ alloys have been found²³ to form diverse crystalline intermetallic phases upon crystallization, all $a-Zr_3RhH_x$ samples with $x \geq 3.6$ irreversibly decompose to form the binary ZrH_x phases. While it was sometimes possible to distinguish between the δ - and ϵ - ZrH_x phases from samples heated to nominally 1000 K, most times the excessive broadening of the x-ray peaks permitted only unequivocal assignment of the (111) d spacing at $2\theta = 32.4^\circ$ that is virtually identical²⁵ for both ZrH_x phases.

The complex crystallization of the partially hydrided $a-Zr_3RhH_x$ samples is demonstrated by the DSC traces in Fig. 5. The XRD measurements (as summarized in Table III) showed that heating foil pieces (i.e., $x = 3.6$ from alloy R-MS-2) or the ungrindable residuals from other $a-Zr_3RhH_x$ preparations produced intermetallic phases previously identified^{12,13} for crystallized original glassy alloys and significantly reduced quantities of ZrH_x . The three exothermic peaks in Fig. 5 for the foil pieces of $a-Zr_3RhH_{3.6}$ imply this particular material consisted of hydrided regions with $x \geq 4$ as well as one or more additional components. However, the absence of a T_{exo} peak near 730 K excludes the presence of unreacted R-MS-2 alloy and suggests that sufficient hydrogen was

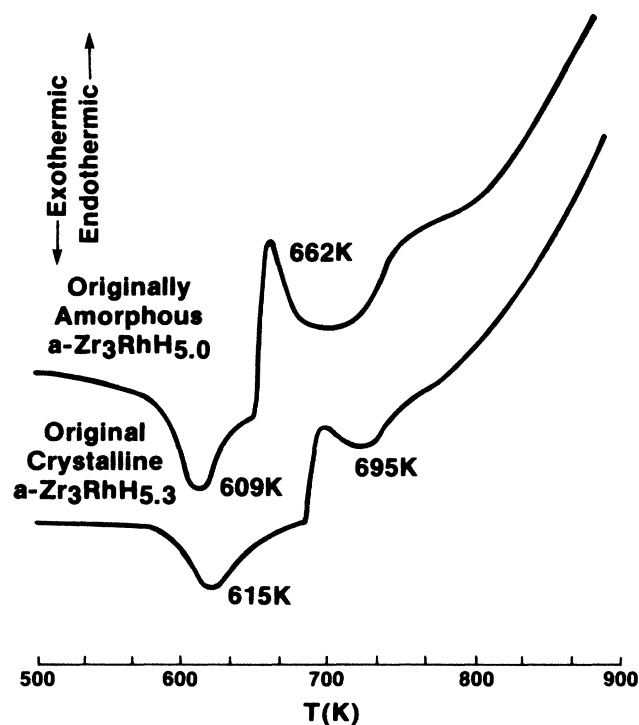


FIG. 6. Comparison of 20-(K/min) DSC traces between amorphous hydrides that were prepared from an initially glassy alloy ($x = 5.0$) and the crystalline Zr_3Rh alloy ($x = 5.3$).

absorbed to alter its crystallization behavior but still permit formation of intermetallic decomposition products.

Although efforts were made to avoid oxygen contamination of $a-Zr_3RhH_x$ during the DSC experiments, the XRD data of the heated samples often indicated the presence of binary (i.e., Zr_3O or ZrO) or ternary (e.g., Zr_6Rh_3O) oxide phases. The amounts of these oxide impurity phases were not quantitatively determined, but are estimated to be as large as several at. % from the relative intensities of the strongest XRD lines. The most likely source of oxygen is the thin oxide surface films that are well known²⁵ to be present on zirconium metal and its hydride. The formation of zirconium suboxides in thermally annealed ZrH_x has been attributed²⁵ to the diffusion of oxygen from this surface oxide layer. The XRD patterns for the heated $a-Zr_3RhH_x$ DSC samples gave no indication of the stable monoclinic ZrO_2 phase—presumably because the DSC measurements were done on hermetically sealed gold cups that contained purified argon gas. Hence, the major oxygen source would be the surface oxide, which should be less

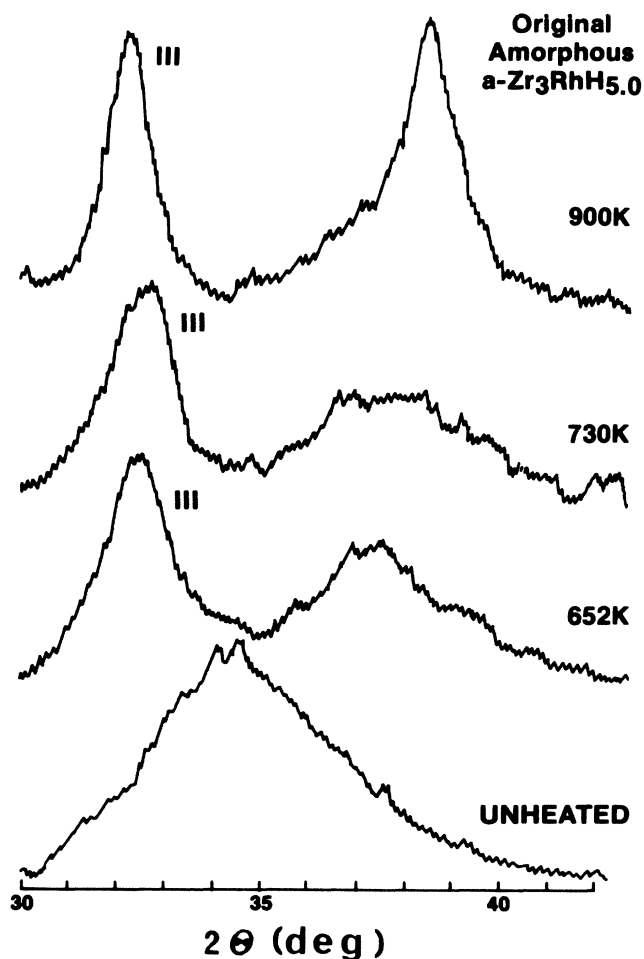


FIG. 7. Portions of the XRD patterns for amorphous $a-Zr_3RhH_{5.0}$ (prepared from originally glassy alloy R-AP-2) after quenching from indicated maximum temperatures during DSC runs.

than 10 nm thick based on past studies.^{12,13,25} This viewpoint is supported by the increase in XRD-detected oxides from $a\text{-Zr}_3\text{RhH}_x$ samples that were exposed as powders to air during handling and other measurements. For example, significant intensities at 2θ values near 39° (which correspond to one of the strongest peaks for ZrO) are clearly evident from the 900-K XRD patterns in Figs. 7 and 8. These peaks do not coincide with the major peaks for the other expected phases formed upon crystallization of $a\text{-Zr}_3\text{RhH}_x$. It is noteworthy that these two samples (i.e., R-AP-2 and R-AP-C) had the longest air exposures in foil and powder forms. Hence, the increased levels of oxides are not surprising.

III. DISCUSSION

A. Hydrogen absorption-amorphization reactions

Until recently, amorphous alloys were almost always prepared by rapid quenching either from the vapor phase or from the melt. In these processes the quenching rates had to be sufficiently high to avoid the nucleation and

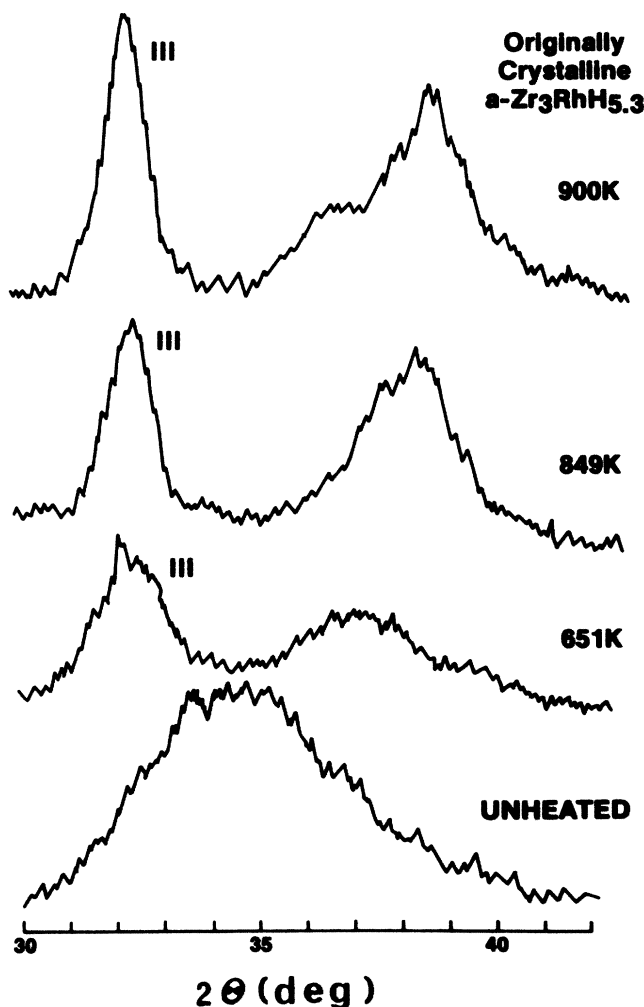


FIG. 8. Portions of the XRD patterns for amorphous $a\text{-Zr}_3\text{RhH}_{5.3}$ (prepared from originally crystalline alloy R-AP-C) after quenching from temperatures during DSC runs.

growth of the more stable crystalline phases. Quenching rates from 10^2 up to 10^{14} K/s can be obtained by different techniques. However, most rapid-quenching procedures restrict the geometrical size of the amorphous sample to below $50\ \mu\text{m}$ in at least one dimension. A solid-state amorphization in which the crystal-to-glass transition occurs at a nominally constant temperature was first found⁸ in the reaction of crystalline $c\text{-Zr}_3\text{Rh}$ with hydrogen gas. The thermodynamic driving force for the structural transformation is the large exothermic heat of mixing between hydrogen and the metal atoms. However, low temperature during this reaction provides kinetic constraints which inhibit chemical segregation of the metal atoms to form more stable crystalline phases. Consequently, SSR permits only a polymorphic transformation with respect to the metal atoms. The very large difference between the mobilities of the hydrogen and metal atoms is the key factor to obtain an amorphous phase by hydrogen absorption. Namely, the more mobile hydrogen atoms can diffuse throughout the alloy to form sufficiently strong chemical bonds that disrupt the local order of the metal atoms. However, the displaced metal atoms are unable to obtain more stable configurations (e.g., crystalline phases) because their mobility is severely limited at these temperatures. Once the amorphous hydride has been produced by a SSR process, it is of particular interest to establish whether these amorphous hydrides have different physical properties (e.g., due to a variation in CSRO) than the hydride produced directly from a rapidly quenched glass. As mentioned in the Introduction, various properties of $a\text{-Zr}_3\text{RhH}_x$ samples prepared under the same conditions from initially crystalline or glassy alloys are found to be essentially identical. These observations support the view that no matter which method was chosen to prepare the amorphous hydride, the microscopic state is unique (within reasonable limits) for the same final composition. Some ramifications of this concept on the role of structure to the characteristics of amorphous metal hydrides will be presented during the remainder of this paper.

The maximum stoichiometries of the amorphous hydrides from the glassy alloys that were produced by melt spinning only reached 70–75 % of the compositions obtained from the anvil-piston-quenched alloys. This difference cannot be readily attributed to incomplete reaction with the MS alloys since they were exposed to hydrogen gas for 4–6 weeks compared to less than 1 week of exposure for the AP alloys. Although differences in the $[\text{Zr}]/[\text{Rh}]$ ratios could cause variations in the maximum hydrogen contents,⁹ a significantly reduced amount of Zr would be necessary. However, this reasoning would also require the MS alloys to have a higher density [since $\rho(\text{Rh}) > \rho(\text{Zr})$], which is contrary to the densities presented in Table I. If anything, the slightly lower densities for the MS glasses compared to that reported²² for $a\text{-Zr}_3\text{Rh}$ would imply that MS-quenched alloys have Zr concentrations greater than 75 at. %, which should have produced higher hydrogen stoichiometries. The two most likely explanations are (1) differences in CSRO between the MS and AP alloys, or (2) effects caused by impurities such as oxygen, which could alter the structure of the alloy or

TABLE III. Summary of the major and minor phases that were identified from powder x-ray-diffraction (XRD) studies on individual DSC samples of $a-Zr_3RhH_x$ after quenching from the maximum heating temperature (T_{max}) to room temperature. The initial XRD patterns on all unheated $a-Zr_3RhH_x$ materials had broad peaks between the 2θ values of 31° and 39° with maxima near 34.5° in 2θ .

x	Source	Sample form	T_{max} (K)	Major phases (structure types)	Minor phases (structure type)	Comments
3.7	R-MS-3	powder	1000	$\epsilon-ZrH_x$, Rh	$\delta-ZrH_x$	not air exposed
< 3.7	R-MS-3	ribbon	1000	$Zr_2Rh(E9_3)$, ZrH_x , Rh		did not grind
3.6	R-MS-2	ribbon	1000	$Zr_2Rh(E9_3)$	ZrH_x	did not grind
4.4	R-MS-2	powder	874	ZrH_x , ZrO (broad peak)		air exposed ^a
4.4	R-MS-2	powder	1000	ZrH_x , Rh		not air exposed
5.0	R-AP-2	powder	900	ZrH_x , ZrO (broad peak)		air exposed
5.0	R-AP-2	powder	800	$ZrH_x(111)^b$ (broad peak)		air exposed
5.0	R-AP-2	powder	730	$ZrH_x(111)^b$ (broad peak)		air exposed
5.0	R-AP-2	powder	652	$ZrH_x(111)^b$ (broad peak)		air exposed
5.1	R-AP-3	powder	899	$\epsilon-ZrH_x$, Rh	ZrO	not air exposed
< 5.1	R-AP-3	ribbon	1000	$Zr_2Rh(C16)$, $\alpha-Zr$	ZrH_x	did not grind (cycled twice to 1000 K)
5.45	R-AP-5	powder	1000	$\epsilon-ZrH_x$, Rh		not air exposed
5.45	R-AP-5	powder	880	ZrH_x , ZrO	Zr_6Rh_3O	air exposed
5.45	R-AP-5	powder	800	$ZrH_x(111)^b$ (broad peak)	Zr_6Rh_3O	air exposed
5.3	R-AP-C	powder	900	ZrH_x , ZrO (broad peak)		air exposed
5.3	R-AP-C	powder	849	$ZrH_x(111)^b$ (broad peak)		air exposed
5.3	R-AP-C	powder	791	$ZrH_x(111)^b$ (broad peak)		air exposed
5.3	R-AP-C	powder	651	$ZrH_x(111)^b$ (broad peak)		air exposed

^aAir exposed denotes material was exposed to air as a powder prior to preparing the DSC sample.

^bOnly this primary peak can be identified.

permit otherwise unfavorable interstitial sites to become occupied (i.e., the occupancy of nominal octahedral sites as found in several oxygen-stabilized crystal structures^{44,45}). It has not been possible from the results available for the present $a-Zr_3RhH_x$ samples to decide whether either factor is actually responsible. However, the recent work of Altounian *et al.*⁴⁶ has shown the important roles of oxygen on the crystallization and other properties of glassy alloys that are Zr rich. Considerable care would be needed to separate the contributions of oxygen contamination from quenching-procedure differences. However, it should be noted that the hydride stoichiometry from the AP-quenched crystalline alloy (R-AP-C) is $x=5.3$, which is within the range for $a-Zr_3RhH_x$ samples from the AP-quenched glassy alloys.

B. Structure and hydrogen-site occupancy

The fundamental issue for SSR is whether it yields the same final arrangement of disordered atoms as the glassy phase formed by rapid quenching. For the $a-Zr_3RhH_x$ system, the first direct evidence of similar amorphous structures was provided by the reduced radial distribution functions $G(r)$ obtained from x-ray-diffraction patterns.^{8,9} Subsequent transmission-electron-microscopy (TEM) studies^{11,16} indicated that fully hydrided crystalline Zr_3Rh alloys had become amorphous, since the TEM images became quite uniform with only minor amounts of

crystalline inclusions. Furthermore, the splittings of the first peak in $G(r)$ were nearly identical⁹ for the hydrides from the initially glassy and initially crystalline alloys. This result was attributed⁹ to a common hydrogen-site occupancy with preference for Zr_4 interstitials. However, more detailed comparisons of local environments for the hydrogen atoms in $a-Zr_3RhH_x$ through analysis of the neutron-scattering radial distribution function^{4,32,33} have not been possible due to limited quantities of suitable samples that have precluded the necessary neutron-diffraction measurements. The INS results for $a-Zr_3RhH_{3.7}$ in Table II are clearly consistent with predominant tetrahedral site occupancy, which is very similar to the other amorphous Zr-based hydrides. Harris *et al.*⁴⁷ have recently proposed that hydrogen atoms occupy equivalent tetrahedral interstitials in all early-late transition-metal glasses. Furthermore, these alloys contain random fivefold rings of tetrahedral sites which are occupied by hydrogen with the blocking of neighboring interstitials. This model has successfully predicted⁴⁷ the trends for maximum $[H]/[M]$ (where M denotes transition metal) ratios as functions of alloy composition in several Zr- and Ti-based amorphous hydrides. However, the possible contributions from CSRO of the metal atoms and probable occupancies of sites with different coordination^{4,32,34} have not been addressed and more quantitative comparisons to the behavior of $a-Zr_3RhH_x$ are probably not warranted without new structural information.

C. Electronic structure and magnetic properties

The crystalline and amorphous $Zr_{1-y}Rh_y$ alloys with $0.20 \leq y \leq 0.35$ are paramagnetic superconductors with T_{sc} usually greater than 4 K (see Refs. 2, 10, 12, 22, 26, and 48). Recent band-theory calculations⁴⁹ as well as photoelectron⁴⁹ and soft-x-ray-emission⁵⁰ spectroscopy measurements have indicated substantial hybridization between the Zr and Rh 4d bands for these alloys. The major effect is a lowering of the Rh states to several eV below the Fermi level such that predominantly Zr states will contribute^{26,49,50} to $N(E_F)$. The theoretical valence-band states for cubic Zr_3Rh were found⁴⁹ to resemble closely the measured photoelectron spectrum from glassy $a-Zr_{75}Rh_{25}$. Mariot *et al.*⁵⁰ have concluded that CSRO is the dominant factor in the electronic structure of Zr_yB_{1-y} alloys and this agreement must arise from very similar local atomic arrangements for the crystalline and

glassy phases. Hence, the variabilities of parameters that depend on $N(E_F)$, such as T_{sc} and $\chi_p(0)$, may be caused by differences in CSRO that arise during preparation of the samples. Of course, unspecified differences in alloy compositions and impurity contents can also produce similar effects. Consequently, there can be no firm explanation for the behavior of the T_{sc} and magnetic parameters for the $a-Zr_3Rh$ alloys in Table I or their differences with results reported in the literature.^{2,22,26} However, the present parameters are considered representative for nominal $a-Zr_3Rh$ glasses.

The absorption of hydrogen has been previously noted⁸⁻¹² to alter the electronic and magnetic properties of $a-Zr_3Rh$ glasses. The influence of hydrogen on several parameters is shown in Fig. 9. Within experimental uncertainties it does not matter whether the glassy alloys were prepared by the MS or AP method. Furthermore, the parameters for $a-Zr_3RhH_{5.3}$ prepared from the crystalline alloy are essentially identical to the values for the samples from originally glassy alloys. Hydrogen addition causes the Debye temperature (Θ_D) to increase while $\chi_p(0)$, T_{sc} , and $N_\gamma(E_F)$ appear to experience linear decreases up to the maximum hydrogen stoichiometry. These three parameters also exhibited^{12,51} similar behavior with hydrogen content for the amorphous $a-Zr_2PdH_x$ system. However, the proton parameter $(T_1 T)^{-1/2}$ is seen in Fig. 9 to be independent of hydrogen content over the limited range $3.7 \leq x \leq 5.3$. It should be noted that the T_{sc} value of 2.95 K for $a-Zr_3RhH_{3.6}$ had been obtained from a resistivity measurement,¹⁰ whereas the specific-heat studies on other portions of this material did not reveal a superconductivity transition above 1.5 K. However, the hydrided ribbons of alloy R-MS-2 were rather inhomogeneous as reflected by their behavior during the DSC-XRD studies (see Fig. 5 for an example). The nonbrittle (i.e., ungrindable) portions produced mostly the crystalline Zr-Rh intermetallics during the DSC runs with only small amounts of the ZrH_x decomposition product. Some of the $a-Zr_3RhH_{3.6}$ ribbon pieces also yielded relatively large amounts of the hydrogen-free intermetallics during the DSC experiments. Hence, the 2.95-K critical temperature probably corresponds to the superconductivity transition for interconnected portions of ribbons with the smaller hydrogen contents. Any lower T_{sc} values from those regions with greater hydrogen contents (i.e., $x > 4.0$) would be unobservable in the resistivity measurements. Since most of the $a-Zr_3RhH_{3.6}$ ribbons were composed of $x > 4.0$ hydride, the specific-heat data did not show the presence of a superconductivity transition around 3.0 K.

Hydrogen absorption is known^{52,53} to substantially alter the electronic structure of the host transition metal. Although the formation of a metal-hydrogen bonding state 5 or 6 eV below the original Fermi level is usually the most dramatic effect, the metal valence band narrows due to the lattice expansion and the Fermi level rises because the metal-hydrogen bond formation does not lower enough states to accept all the electrons brought by the hydrogen atoms. Because the electronic states near the Fermi level for $a-Zr_{1-y}Rh_y$ are dominated by the Zr d band,^{26,49,50} the interactions of hydrogen with its zirconi-

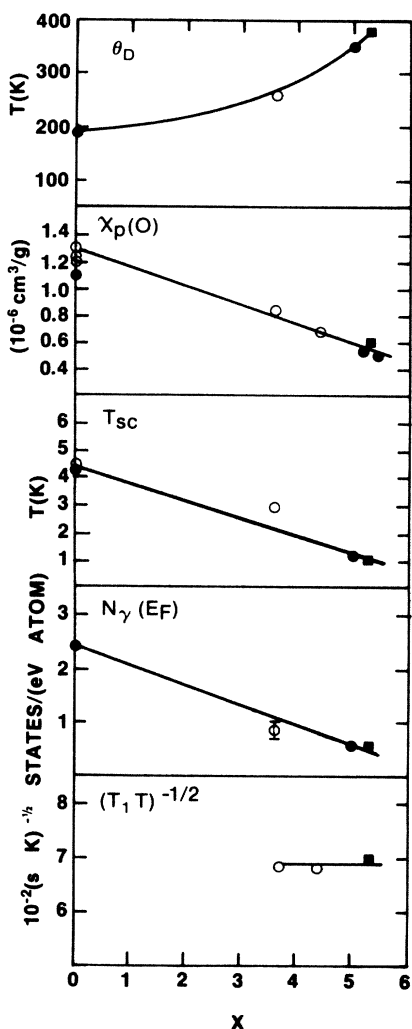


FIG. 9. Stoichiometry dependencies of several electrical, magnetic, and thermal properties of $a-Zr_3RhH_x$ (see text for identification of parameters). Open symbols represent melt-spun (MS) alloys and solid symbols correspond to anvil-piston- (AP-) quenched alloys.

um neighbors will modify $N(E_F)$. The electron parameters T_{sc} , $\chi_p(0)$, and $N_\gamma(E_F)$ in Fig. 9 indicate an approximately linear decrease with the absorption of hydrogen. This behavior has been mainly attributed^{10–12} to reductions in the bare density of Fermi-level states. However, a more detailed analysis of the electronic properties of $a-Zr_2PdH_x$ has recently shown⁵¹ that the decrease in the phonon-dressed $N(E_F)$ is partially caused by a decrease in the electron-phonon-coupling constant λ . The renormalized bare density of states for $a-Zr_2PdH_x$ still decreased slightly with increasing hydrogen concentration, but the $N(E_F)$ calculated within the free-electron model remained constant. Although $\chi_p(0)$ and $N_\gamma(E_F)$ give the dressed density of states, the NMR parameters correspond to the bare states.^{27,28} Hence, the constant proton $(T_1 T)^{-1/2}$ values in Fig. 9 imply that $N(E_F)$ is approximately constant—at least for hydrogen contents between $x = 3.7$ and 5.3.

The behavior of the $a-Zr_3RhH_x$ system can be considered analogous to the previously analyzed⁵¹ electronic properties of $a-Zr_2PdH_x$. The T_{sc} values for $a-Zr_2PdH_x$ were found to decrease with increasing hydrogen content up to $[H]/[M] \approx 0.5$ and stays constant up to $[H]/[M] \approx 1.1$. As previously described, the specific-heat measurements for $a-Zr_3RhH_{3.6}$ had shown no indication for $T_{sc} > 1.5$ K, although the effective hydrogen content for most of this material is actually slightly greater than $x = 4.0$. Since resistivity measurements⁹ gave $T_{sc} \approx 1.1$ K for $x \geq 5.0$, the superconductivity transition temperatures are probably approximately constant over the hydrogen range $4.0 \leq x \leq 5.5$. These results are consistent with the proton $(T_1 T)^{-1/2}$ parameters. From the arguments of Kullik *et al.*,⁵¹ the decrease in the dressed $N(E_F)$ values from the $\chi_p(0)$ and $N_\gamma(E_F)$ parameters are dominated by a decrease in λ . If the Θ_D and T_{sc} values in Table II are inserted into the well-known McMillan equation⁵⁴ with the estimated² Coulomb pseudopotential $\mu^* = 0.13$, $\lambda = 0.7$ for the alloy *R-AP-1* and decreases to 0.4 for the two amorphous hydrides with $x = 5.0$ and 5.3. Hence, the expected λ decrease is obtained over the total hydrogen stoichiometry range. At higher hydrogen concentrations, less stable interstitial sites should become occupied in $a-Zr_3RhH_x$ as indicated by the neutron experiments^{4,33} on other Zr-based glassy hydrides. The T_{sc} appears to remain constant⁵¹ as these new sites are filled. Perhaps, the electron-phonon coupling changes⁵¹ or the nature of the electronic states becomes more *s*-like as suggested by proton NMR studies⁶ on Zr_2PdH_x . However, the actual process is presently unclear. The apparent hydrogen content for a constant T_{sc} occurs near $[H]/[M] \approx 0.8$ for $a-Zr_3RhH_x$ compared to $[H]/[M] \approx 0.5$ found in $a-Zr_2PdH_x$. The probable reason is simply the higher Zr content for $a-Zr_3Rh$, which gives more Zr_4 sites to be occupied before the presumably less stable sites will start to contribute.

D. Thermal stabilities of $a-Zr_3RhH_x$

Since the glassy alloys are metastable, they usually undergo exothermic irreversible crystallization reactions.⁵⁵

Although these transitions are occasionally polymorphic, most amorphous solids experience phase segregation or decomposition where the final products correspond to the equilibrium phase diagram for the combination of elements under investigation. As described in Sec. II F, all of the glassy $a-Zr_3RhH_x$ samples can be converted into crystalline phases. Although the hydrogen-free $a-Zr_3Rh$ alloys do not follow identical crystallization paths,²³ all hydrided samples with $x > 3.6$ produce binary ZrH_x as the major product identified by XRD. ZrH_x has been found following the crystallization of all other Zr-based amorphous hydrides^{5,6,13,18,56} when $[H]/[Zr] > 0.5$. However, the various glasses often produced very different Zr-depleted crystalline phases, as discussed by Cantrell and Bowman.¹⁵ The $a-Zr_3RhH_x$ samples with $x \geq 3.6$ show the presence of free Rh metal only in samples heated above 900 K. Presumably, the dimensions of the Rh particles formed during the crystallization-decomposition transition are sufficiently small (i.e., ≤ 10 nm) to give very broad XRD peaks that cannot be resolved in the XRD patterns until enough grain growth had occurred by heating to these higher temperatures.

The effects of hydrogen concentration on the peaks of the exothermic and endothermic transitions observed from all the $a-Zr_3RhH_x$ samples are shown in Fig. 10. From the XRD data on samples cooled from temperatures above T_{exo} , the exothermic transitions correspond

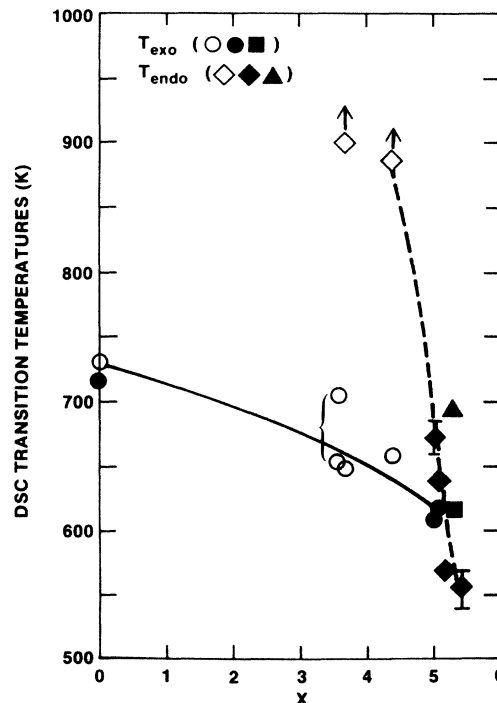


FIG. 10. Effects of hydrogen concentrations on the exothermic (T_{exo}) and endothermic (T_{endo}) peaks obtained during DSC runs at 20 K/min on $a-Zr_3RhH_x$ samples. The symbols ■, ▲ correspond to an amorphous hydride that was produced from the originally crystalline alloy *R-AP-C*. Open symbols represent melt-spun (MS) $a-Zr_3Rh$ alloys, while solid symbols represent anvil-piston- (AP-) quenched alloys.

to crystallization of the amorphous alloys or formation of crystalline ZrH_x . T_{exo} decreases from above 700 K for the original glassy alloys to below 620 K for the amorphous hydrides with $x \geq 5.0$. The three T_{exo} values for the $a-Zr_3RhH_{3.6}$ sample reflect contributions from two or more distinct regions with different hydrogen contents. When $x < 4.0$, T_{endo} exceeds 900 K. However, the endotherms rapidly occur at lower temperatures for $x > 4.4$ until the exothermic peak is completely masked in the endothermic peaks from the $a-Zr_3RhH_{5.45}$ sample. Although the DSC experiments were performed on sealed samples with minimum free volumes to restrict the escape of hydrogen gas, the endothermic transitions correspond to the evolution of hydrogen gas from the hydride. Since T_{endo} decreases rapidly above $x = 4.4$, the hydrogen must have come from the less stable interstitial sites that are occupied with decreasing binding energy as the stoichiometry increases. Yeh and Cotts¹⁸ have recently reported a very similar trend for the endothermic peaks in their DSC studies of $a-Zr_{1-y}Rh_yH_x$.

The T_{exo} peak for $a-Zr_3RhH_{5.3}$, which was prepared from the initially crystalline alloy, is nearly identical to the values for samples with $x \geq 5.0$ that were hydrided glassy alloys. Furthermore, the exothermic heats of transition are also equal within experimental accuracy. Although these results cannot prove that these amorphous hydrides are indistinguishable on a microscopic scale,

they support this interpretation since the final crystallization products are the same as noted in Table III. While metastable crystalline hydrides can have exothermic transitions as were seen in the $Ti_{1-y}Cu_yH_x$ system,⁵⁷ different heats of transitions are also anticipated and were observed. Hence, the DSC-XRD experiments provide additional evidence that an essentially unique form of amorphous state has been created in $a-Zr_3RhH_x$ irrespective of the structure of the initial alloy.

ACKNOWLEDGMENTS

We wish to thank X.-L. Yeh and W. E. Tadlock for preparation of the hydrides, A. Attalla for his help with the samples and some of the NMR measurements, and J. E. Wagner and D. E. Etter for assistance with the DSC measurements. The interest and support of W. L. Johnson has been appreciated. Portions of this work were performed at Monsanto Research Corporation—Mound Laboratory, which is operated for the U.S. Department of Energy under Contract No. DE-AC04-76-DP00053. Sandia National Laboratories are supported by the U.S. Department of Energy under Contract No. DE-AC04-76DP00789. The support by the Deutsche Forschungsgemeinschaft, under Sonderforschungsbereich SFB-126, is gratefully acknowledged. This work was partially supported by the Aerospace Sponsored Research Program.

¹See, for example, articles and references in *Hydrogen in Disordered and Amorphous Solids*, edited by G. Bambakidis and R. C. Bowman, Jr. (Plenum, New York, 1986).

²A. Inoue, K. Matsuzaki, T. Masumoto, and H. S. Chen, *J. Mater. Sci.* **21**, 1258 (1986).

³R. C. Bowman, Jr., M. J. Rosker, and W. L. Johnson, *J. Non-Cryst. Solids* **53**, 105 (1982).

⁴K. Suzuki, *J. Less-Common Met.* **89**, 183 (1983).

⁵S. M. Fries, H.-G. Wagner, S. J. Campbell, U. Gonser, N. Blaes, and P. Steiner, *J. Phys. F* **15**, 1179 (1985).

⁶R. C. Bowman, Jr., W. L. Johnson, A. J. Maeland, and W.-K. Rhim, *Phys. Lett. A* **94**, 181 (1983); R. C. Bowman, Jr., A. Attalla, A. M. Maeland, and W. L. Johnson, *Solid State Commun.* **47**, 779 (1983); R. C. Bowman, Jr., J. S. Cantrell, A. Attalla, D. E. Etter, B. D. Craft, J. E. Wagner, and W. L. Johnson, *J. Non-Cryst. Solids* **61&62**, 649 (1984).

⁷R. C. Bowman, Jr., in *Hydrogen in Disordered and Amorphous Solids*, Ref. 1, p. 237.

⁸X. L. Yeh, K. Samwer, and W. L. Johnson, *Appl. Phys. Lett.* **42**, 242 (1983).

⁹K. Samwer and W. L. Johnson, *Phys. Rev. B* **28**, 2907 (1983).

¹⁰R. C. Bowman, Jr., J. S. Cantrell, E. L. Venturini, R. Schulz, J. E. Wagner, A. Attalla, and B. D. Craft, in *Rapidly Quenched Metals*, edited by S. Steeb and H. Warlimont (Elsevier, Amsterdam, 1985), p. 1541.

¹¹J. Tebbe, K. Samwer, and R. Schulz, in *Rapidly Quenched Metals*, Ref. 10, p. 1581.

¹²E. L. Venturini, R. C. Bowman, Jr., and J. S. Cantrell, *J. Appl. Phys.* **57**, 3542 (1985).

¹³J. E. Wagner, R. C. Bowman, Jr., and J. S. Cantrell, *J. Appl. Phys.* **58**, 4573 (1985).

¹⁴K. Samwer, in *Hydrogen in Disordered and Amorphous Solids*, Ref. 1, p. 173.

¹⁵J. S. Cantrell and R. C. Bowman, Jr., *Mater. Res. Symp. Proc.* **80**, 105 (1987).

¹⁶X. L. Yeh, Ph.D. thesis, California Institute of Technology, 1986 (unpublished).

¹⁷X. L. Yeh, W. L. Johnson, J. Y. Tang, and C. R. Shi, *Mater. Res. Soc. Symp. Proc.* **58**, 63 (1986).

¹⁸X. L. Yeh and E. J. Cotts, *J. Mater. Res.* **2**, 173 (1987).

¹⁹R. Schwarz and W. L. Johnson, *Phys. Rev. Lett.* **51**, 415 (1983).

²⁰M. Atzmon, J. D. Verhoeven, E. D. Gibson, and W. L. Johnson, *Appl. Phys. Lett.* **45**, 1052 (1984).

²¹R. C. Bowman, Jr. (unpublished).

²²A. J. Drehman and W. L. Johnson, *Phys. Status Solidi A* **52**, 499 (1979).

²³J. S. Cantrell, J. E. Wagner, and R. C. Bowman, Jr., *J. Appl. Phys.* **57**, 545 (1985).

²⁴A. Attalla and R. C. Bowman, Jr., in *Analytical Spectroscopy*, edited by W. S. Lyon (Elsevier, Amsterdam, 1984), p. 363.

²⁵R. C. Bowman, Jr., B. D. Craft, J. S. Cantrell, and E. L. Venturini, *Phys. Rev. B* **31**, 5604 (1985).

²⁶H.-J. Eifert, B. Elschner, and K. H. J. Buschow, *Phys. Rev. B* **29**, 2905 (1984).

²⁷R. C. Bowman, Jr., *Hyperfine Interact.* **24-26**, 583 (1985).

²⁸G. C. Carter, L. H. Bennett, and D. J. Kahan, *Metallic Shifts in NMR* (Pergamon, Oxford, 1977).

²⁹D. R. Torgeson, L.-T. Lu, T.-T. Phua, R. G. Barnes, D. T. Peterson, and E. F. W. Seymour, *J. Less-Common Met.* **104**, 79 (1984).

³⁰D. K. Ross, P. F. Martin, W. A. Oates, and R. Khoda-

- Bakhsh, Z. Phys. Chem. Neue Folge **114**, 221 (1980).
- ³¹R. Hempelmann and J. J. Rush, in *Hydrogen in Disordered and Amorphous Solids*, Ref. 1, p. 283.
- ³²K. Kai, S. Ikeda, T. Fukunaga, N. Watanabe, and K. Suzuki, *Physica* **120B**, 342 (1983).
- ³³K. Suzuki, N. Hayashi, Y. Tomizuka, T. Fukunaga, K. Kai, and N. Watanabe, *J. Non-Cryst. Solids* **61&62**, 637 (1984).
- ³⁴J. J. Rush, J. M. Rowe, and A. J. Maeland, *J. Phys. F* **10**, L283 (1980).
- ³⁵A. Magerl, J. J. Rush, and J. M. Rowe, *Phys. Rev. B* **33**, 2093 (1986).
- ³⁶A. Williams, J. Eckert, X. L. Yeh, M. Atzmon, and K. Samwer, *J. Non-Cryst. Solids* **61&62**, 643 (1984).
- ³⁷H. Kaneko, T. Kajitani, M. Hirabayashi, M. Ueno, and K. Suzuki, *J. Less-Common Met.* **89**, 237 (1983).
- ³⁸J. J. Rush, R. C. Bowman, Jr., and A. J. Maeland (unpublished).
- ³⁹J. G. Couch, O. K. Harling, and L. C. Clune, *Phys. Rev. B* **4**, 2675 (1971).
- ⁴⁰R. C. Bowman, Jr., E. L. Venturini, and W.-K. Rhim, *Phys. Rev. B* **26**, 2652 (1982).
- ⁴¹Although Williams *et al.* (Ref. 36) give their sample stoichiometry as $Zr_2PdH_{3.51}$ from the weight gain after reaction with hydrogen, NMR spin counts on a powdered portion of this material gave $x = 2.95 \pm 0.14$. Hence this latter value should be preferred since the presence of extraneous oxygen (Ref. 36) is probably responsible for the higher stoichiometry originally quoted.
- ⁴²K. Samwer and H. v. Lohneysen, *Phys. Rev. B* **26**, 107 (1982).
- ⁴³In this paper the heats of transition are referenced to 1 g-at. (i.e., 6.023×10^{23} metal atoms) to facilitate comparisons with other alloy systems where the compositions are different. In contrast, these values in previous papers (Refs. 13, 15, and 23) were referenced to formula weights [i.e., $4(6.023 \times 10^{23})$ metal atoms for $a-Zr_3RhH_x$].
- ⁴⁴F. J. Rotella, H. E. Flotow, D. M. Gruen, and J. D. Jorgeson, *J. Chem. Phys.* **79**, 4522 (1983).
- ⁴⁵A. J. Maeland, *J. Less-Common Met.* **89**, 173 (1983).
- ⁴⁶Z. Altounian, E. Battalla, J. O. Strom-Olsen, and J. L. Walter, *J. Appl. Phys.* **61**, 149 (1987).
- ⁴⁷J. H. Harris, W. A. Curtin, and M. A. Tenhover, *Bull. Am. Phys. Soc.* **32**, 569 (1987); *Phys. Rev. B* **36**, 5784 (1987).
- ⁴⁸R. Kuentzler and R. M. Waterstrat, *Solid State Commun.* **54**, 517 (1985).
- ⁴⁹V. L. Moruzzi, P. Oelhafen, A. R. Williams, R. Lapka, J.-J. Güntherodt, and J. Kubler, *Phys. Rev. B* **27**, 2049 (1983).
- ⁵⁰J.-M. Mariot, C. F. Hague, P. Oelhafen, and H.-J. Güntherodt, *J. Phys. F* **16**, 1197 (1986).
- ⁵¹M. Kullik, G. von Minnigerode, and K. Samwer, *Z. Phys. B* **60**, 357 (1985).
- ⁵²L. Schlapbach, S. Hufner, S. Buchler, and T. Riesterer, *J. Less-Common Met.* **130**, 301 (1987).
- ⁵³T. Riesterer, *Z. Phys. B* **66**, 441 (1987).
- ⁵⁴W. L. McMillan, *Phys. Rev.* **167**, 331 (1968).
- ⁵⁵U. Koster and U. Herold, in *Glassy Metals*, edited by J.-J. Güntherodt and H. Beck (Springer, Berlin, 1981), p. 225.
- ⁵⁶K. Dini and R. A. Dunlap, *J. Phys. F* **15**, 273 (1985).
- ⁵⁷R. J. Furlan, G. Bambakidis, J. S. Cantrell, and R. C. Bowman, Jr., *J. Less-Common Met.* **116**, 375 (1986).